

# Development of a Conceptual-Level Thermal Management System Design Capability in OpenConcept

**Benjamin J. Brelje**

**John P. Jasa**

**Joaquim R. R. A. Martins**

University of Michigan Department of Aerospace Engineering  
Francois-Xavier Bagnoud Building  
1320 Beal Ave.  
Ann Arbor, MI 48109  
UNITED STATES

[bbrelje@umich.edu](mailto:bbrelje@umich.edu)

**Justin S. Gray**

NASA Glenn Research Center  
21000 Brookpark Rd.  
Cleveland, OH 44135  
UNITED STATES

*Keywords: “Integrated Thermal Regulation and Control Systems”*

## **ABSTRACT**

*Thermal management constraints will be a key consideration for hybrid- and all-electric aircraft designers. While airplane sizing and multidisciplinary analysis and design optimization (MDAO) tools with support for electrification have been developed, most of these tools do not support thermal analysis and almost all are closed-source or otherwise unavailable to the broader research community. In this paper, we introduce thermal analysis extensions to OpenConcept, which is a toolkit for conceptual-level design optimization of aircraft with unconventional propulsion built using the OpenMDAO framework. We provide implementation details for an open-source, physics-based thermal management system (TMS) analysis and design capability in OpenConcept. We develop governing equations for component-based, air-cooled and liquid-cooled thermal management systems. We detail the implementation of thermal mass, heat sink, heat exchanger, incompressible duct, coolant loop, and refrigeration components with analytic derivatives in OpenMDAO. We also describe a method for computing time-dependent electrical component temperatures throughout a mission profile using OpenMDAO’s Newton solver. To illustrate thermal effects, we consider a tradespace study on a Beech King Air with a series hybrid electric propulsion system. We optimize the aircraft for minimum fuel burn with and without thermal constraints and TMS penalties. The optimizer sizes the TMS components to keep component temperatures within limits while minimizing the associated fuel burn penalty. We demonstrate reasonable robustness of the thermal model across a broad range of aircraft designs and compare the optimal designs with and without thermal constraints and TMS penalties.*

## **1.0 INTRODUCTION**

Electric aircraft propulsion has emerged as a widely popular topic in the aerospace research community. The initial design studies quickly identified shortcomings in existing aircraft analysis techniques and tools. Several analysis codes with similar levels of fidelity for integrating energy used over a mission have been announced [1–10], but only one has been open-sourced or made publicly available [10]. There is also significant duplication of effort in the research community, particularly within the area of electrical system

modeling and mission analysis. Despite multiple industry and government studies demonstrating the need to include thermal constraints in analysis and optimization at the conceptual level [1, 2, 11, 12], no publicly-available electric propulsion mission analysis and sizing code supports thermal analysis.

We have recently introduced OpenConcept ([openconcept.readthedocs.io](https://openconcept.readthedocs.io)) a new, open source, conceptual design and optimization toolkit for aircraft with electric propulsion [13]. OpenConcept consists of three parts: a library of simple conceptual-level models of common electric propulsion components; a set of analysis routines necessary for aircraft sizing and optimization; and several example aircraft models. All of OpenConcept’s codes compute derivatives efficiently and accurately, enabling the use of OpenMDAO’s Newton solver [14], as well as gradient-based optimization methods.

In prior work, we performed a case study involving the electrification of existing turboprop airplanes [13]. We defined a series-hybrid electric propulsion architecture for the Beechcraft King Air and solved more than 750 multidisciplinary design optimization (MDO) problems for different combinations of range and specific energy (Fig. 1-1), demonstrating that OpenConcept is a flexible and efficient way of doing trade space exploration for unconventional propulsion architectures.

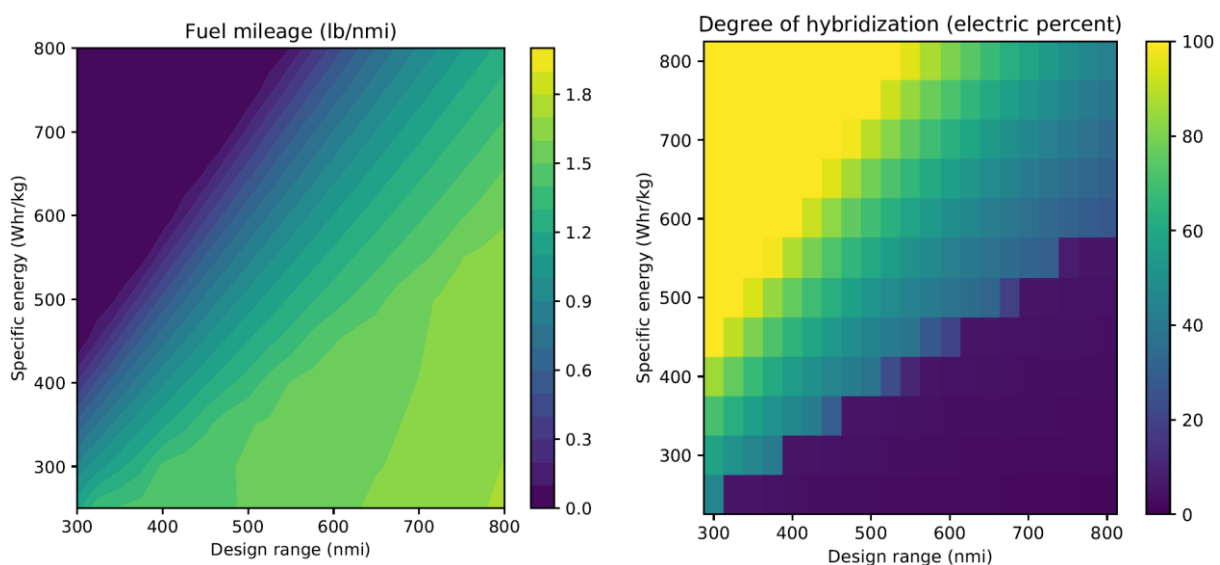


Figure 1-1: Minimum fuel burn MDO results from our previous work [13]

In our previous version of OpenConcept, conceptual-level models of heat exchangers, heat sinks, coolant loops, heat pumps, and associated flow paths had not yet been developed, and thermal constraints were not imposed for the results shown Fig. 1-1 [13].

In the broader literature, a few attempts at physics-based thermal management system (TMS) modeling of electric aircraft have been made [15–17], but none of the codes have been publicly released or open-sourced. The primary purpose of this paper is to describe our thermal modeling approach and the implementation of the thermal components. We then isolate the effect of thermal constraints by repeating the King Air tradespace study with TMS design variables.

## 2.0 THERMAL MANAGEMENT SYSTEM MODELING

The thermal management system of an electric (or hybrid-electric) aircraft removes waste heat from the electronic components. Unlike conventional turbine-powered aircraft, electric aircraft have two features that

significantly increase the magnitude of the thermal management challenge. First, while turbine engines have lower efficiency, they exhaust their waste heat to the free stream and away from the aircraft. In contrast, Ohmic resistance and eddy current losses in electrical components generate heat within the components themselves and require designers to provide a way to carry away the heat. Second, electrical components must be kept at fairly low temperatures to operate properly, which means their waste heat is “low-quality” and much more difficult to reject from the components.

There are two general design approaches to aircraft thermal management systems: direct air cooling and liquid cooling. The air-cooled approach uses carefully-designed heat sinks to enhance convection from each electrical component to freestream air. The X-57 Maxwell demonstrator uses this approach [15, 18]. An advantage of this approach is system simplicity and reliability. A major disadvantage is that each electrical component requires direct access to an air flow path, increasing configuration complexity and potentially increasing drag as well. The liquid-cooled approach uses coolant loops to transfer heat from the electrical components throughout the aircraft to a heat exchanger that can reject the heat to the air [11]. This approach likely reduces the number of cooling air ducts. It also provides the option to use a refrigeration cycle or a fan to improve heat rejection at low airspeed. However, the liquid cooling architecture is a more complex system design (with more failure modes and moving parts). Some aircraft may use a combination of liquid cooling and direct air cooling. A notional liquid-cooled TMS architecture is illustrated in Fig. 2-1. The following subsections detail the physics and numerical methods governing each component of the TMS as modeled in OpenConcept.

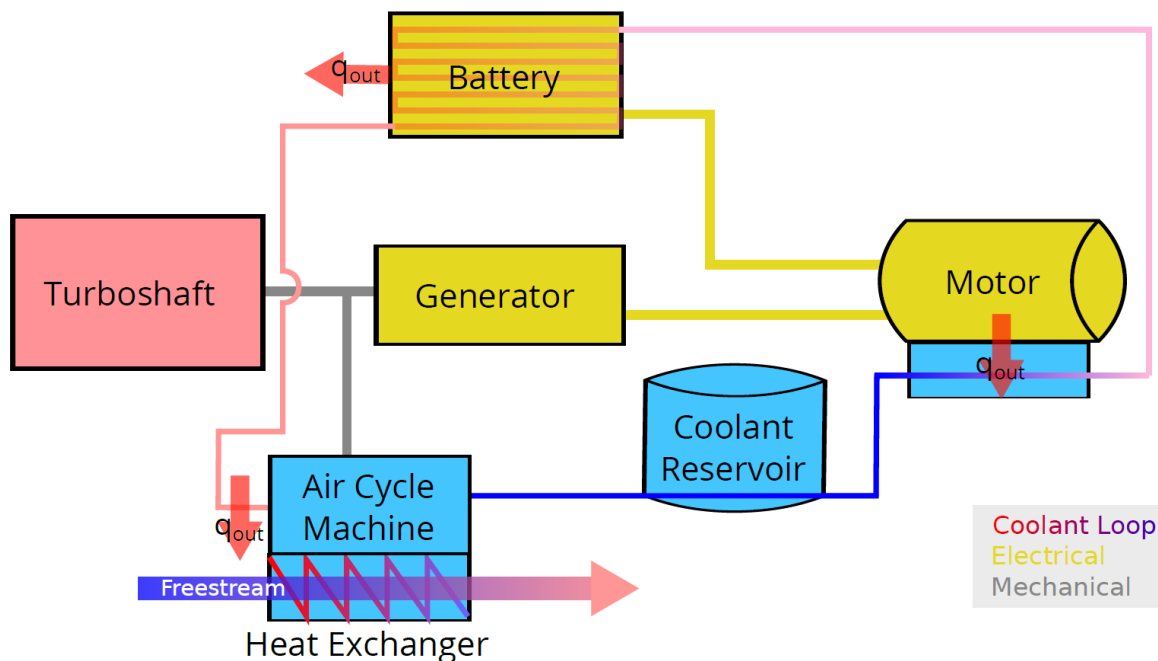


**Figure 2-1: Example of liquid-cooled thermal management system architecture**

## 2.1 Component Temperatures

All existing OpenConcept electrical components (SimpleMotor, SimpleGenerator, SOCBattery) have a `heat_out` output variable that computes the heat generation rate of the component at the current operating point. The components produce heat as a fraction of operating power via an assumed efficiency loss, though higher-fidelity heating models could be used in the future. If the user wishes to track thermal

constraints on a component, they must add an instance of a `ThermalComponent` to the model and properly connect it to the electrical component's heat output. The user can either solve for quasi-steady temperatures at each analysis point, or time-accurate temperatures.

The quasi-steady formulation relies on OpenMDAO's Newton solver to compute component temperatures that satisfy conservation of energy. The implicit problem, implemented in the `ThermalComponentMassless` class, is:

$$\begin{aligned} &\text{compute } T_{\text{comp}} \\ &\text{such that } R(T_{\text{comp}}) = q_{\text{comp}} - q_{\text{out}} = 0 \end{aligned} \quad (1)$$

where  $T_{\text{comp}}$  is the component temperature,  $q_{\text{comp}}$  is the heat generation rate of the electrical component, and  $q_{\text{out}}$  is the instantaneous heat rejection rate due to cooling. The heat rejection rate is computed as a function of the component temperature  $T_{\text{comp}}$  and a number of other heat transfer parameters (introduced in Section 2-2).

$$q_{\text{out}} = q(T_{\text{comp}}, \dots) \quad (2)$$

The quasi-steady formulation becomes less accurate as the thermal mass increases. Even lightweight aerospace-grade electrical components have a significant thermal mass, and at low-speed conditions (such as the beginning of the takeoff roll), neglecting thermal mass is likely to result in unrealistic high temperatures and drive oversized TMS designs. Therefore, we recommend using a time-accurate model, which can be expressed as

$$\frac{dT_{\text{comp}}}{dt} = \frac{q_{\text{comp}} - q(T_{\text{comp}}, \dots)}{m_{\text{comp}} c_p} \quad (3)$$

$$T_{\text{comp}} = \int_{t_0}^{t_f} \frac{dT_{\text{comp}}}{dt} dt \quad (4)$$

where  $q_{\text{comp}}$  is the heat generated by the electrical component. Equations (3) and (4) depend on each other and hence form an implicit cycle that can be solved in OpenMDAO using its built-in Newton solver.

The rate  $dT_{\text{comp}} / dt$  is computed by the `ThermalComponentWithMass` component. A numerical scheme is required to compute the time integral in Equation (4). Our `Integrator` component provides the user a choice of a fourth-order accurate Simpson's Rule discretization (as previously described [13]), or the BDF3 discretization, which sacrifices some accuracy for better stability on stiff systems. Both of these integration methods are solved implicitly in vectorized form all-at-once using the Newton solver (without time marching). This means that the time integration and the implicit ODE are solved simultaneously as one coupled nonlinear system. The user must specify an initial component temperature, usually based on ambient conditions. Unlike the quasi-steady problem, the accuracy of the temperature profile depends on the time step chosen. A smaller time step increases the size of the OpenMDAO implicit problem that needs to be solved and increases the computation time.

## 2.2 Component-Fluid Heat Transfer

So far, we have not addressed the question of how to compute  $q_{\text{out}}$  from each component, which represents the convective heat transfer rate from the component to a fluid stream. For a liquid-cooled component, the fluid stream is a coolant like propylene glycol, whereas for an air-cooled component the fluid stream comes

from freestream air. In nearly every case, designers use enhanced heat transfer surfaces, such as microchannels or finned heat sinks. The `ConstantSurfaceTemperatureColdPlate_NTU` component implements a microchannel cold plate and is a reasonable choice for liquid-cooled and air-cooled applications. We assume that the thermal conductivity of the electrical component is large relative to the cooling fluid resulting in a constant channel surface temperature in the streamwise direction. We further assume that the aspect ratio of each channel is large and thus approximates the local heat transfer properties using the theoretical result for infinite parallel plates. The convective heat transfer coefficient can be computed as

$$h = \frac{\text{Nu } k}{d_h}, \quad (5)$$

where  $\text{Nu}$  is the Nusselt number (which is set to 7.54 by default for constant temperature infinite parallel plates [19]),  $k$  is the thermal conductivity of the fluid, and  $d_h$  is the hydraulic diameter of the channel. For a high aspect ratio channel,

$$d_h = \frac{2wh}{w + h} \quad (6)$$

where  $w$  is the fluid channel width and  $h$  is the fluid channel height. We neglect entrance effects for this high aspect ratio microchannel. For air cooled applications using finned heat sinks, the user may wish to modify the heat transfer coefficient to account for fin efficiency. To compute the overall heat transfer, we first need to compute the heat transfer surface area as

$$A = 2L(w + h)N_{\text{parallel}}, \quad (7)$$

where  $A$  is the overall heat transfer surface area,  $L$  is the length of the microchannel in the fluid flow direction, and  $N_{\text{parallel}}$  is the total number of individual microchannels.

Given these convective properties, we compute the actual heat transfer using the NTU-effectiveness method [19], which is typically used for fluid-fluid heat exchangers where both fluids change temperature during the exchange. In this work, we assume that the heat transfer capability of the conductive component body is “infinite” for the purposes of the NTU-effectiveness method. Therefore, the heat transfer capacity of the cold plate is governed solely by the coolant material properties and flow rate. The heat transfer capacity is computed as:

$$C_{\min} = \dot{m}_{\text{coolant}} c_{p,\text{coolant}}, \quad (8)$$

where  $\dot{m}_{\text{coolant}}$  is the coolant mass flow rate through the entire cold plate (not just a single channel) and  $c_{p,\text{coolant}}$  is the coolant’s specific heat capacity. The number of thermal units (NTU) is computed as

$$\text{NTU} = \frac{Ah}{C_{\min}}, \quad (9)$$

and heat transfer effectiveness is

$$\epsilon = 1 - e^{-NTU} \quad (10)$$

Finally, we can compute the heat transfer as

$$q_{out} = \epsilon C_{min}(T_{comp} - T_{coolant,in}), \quad (11)$$

and the coolant outlet temperature as

$$T_{coolant,out} = T_{coolant,in} + \frac{q_{out}}{C_{min}}. \quad (12)$$

The user is responsible for setting reasonable values for channel geometry ( $L$ ,  $w$ ,  $h$ ,  $N_{parallel}$ ) so that the channel flow is laminar and the infinite parallel plate assumption remains reasonable, and for ensuring that the component has sufficient material volume to accommodate the cooling channels. This analysis also assumes that the cooling channel weight is accounted for in the all-up weight of the component, which may not be the case for air-cooled external heat sinks. In practice, we have found that the thermal resistance of the component-liquid heat transfer is much smaller than for the liquid-air main heat exchanger, and that aircraft design problems are not that sensitive to cold plate channel design parameters. However, the detailed design of internal cooling channels in electrical components is a challenging problem in its own right.

### 2.3 Fluid-Fluid Heat Transfer

After heat from electrical components is transferred into the liquid coolant loop via the cold plate, the heat must be rejected to the atmosphere. A reasonable choice for accomplishing this is a ducted compact heat exchanger. Like the cold plate component above, we use the NTU-effectiveness method to compute the heat transfer rate,

$$q = \epsilon \frac{UA_{overall}}{NTU} (T_{in,h} - T_{in,c}), \quad (13)$$

where  $UA_{overall}$  is the overall heat transfer coefficient times the corresponding heat transfer area,  $T_{in,h}$ ,  $T_{in,c}$  are the fluid inlet temperatures, the number of thermal units is computed as

$$NTU = \frac{UA_{overall}}{C_{min}}, \quad (14)$$

and the heat transfer effectiveness is

$$\epsilon = \Phi \left( NTU, \frac{C_{min}}{C_{max}} \right), \quad (15)$$

where  $C_{min}$ ,  $C_{max}$  are the maximum and minimum values of the fluid heat transfer capacity  $\dot{m} c_p$  for the hot and cold sides, and  $\Phi$  is an analytical or empirical function that depends on the flow arrangement of the heat exchanger (for example, crossflow) [20].

For this study, we use crossflow plate-fin heat exchangers with offset strip fin geometry as described by Jasa et al. [21]. Offset strip fin heat exchangers are considered “compact” heat exchangers with high heat transfer

to surface area rates [20]. The geometric design of a heat exchanger varies to satisfy heat transfer, pressure loss, weight, and volume requirements. Figure 2.3-1 illustrates a cross section of offset strip fin channels along with a commonly-used geometric parameterization.

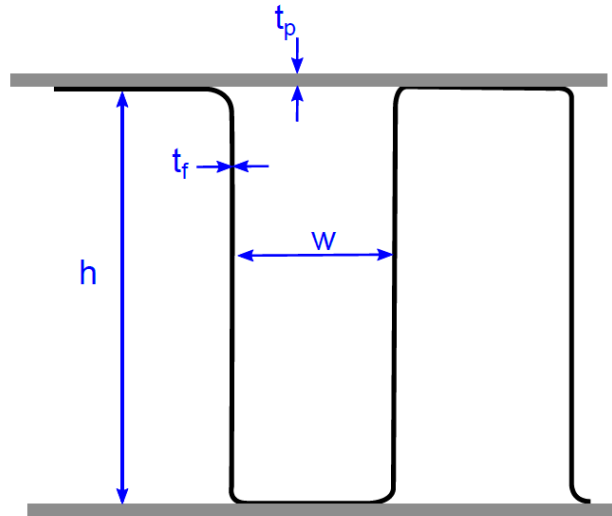


Figure 2.3-1: Cross-sectional geometry of the offset strip fin heat exchanger [21]

We use an empirical relation from Manglik and Bergles [22] to compute heat transfer and pressure loss specific to the offset strip fin configuration. By default, OpenConcept's HXGroup component uses geometric parameters representative of a air-liquid heat exchanger, with cold-side channel width and height 1 mm, and hot-side channel width 14 mm by 1.35 mm.

## 2.4 Fluid Reservoir

Any liquid cooling system needs a reservoir. The thermal mass of the fluid in the reservoir may significantly affect peak temperatures. We assume perfect mixing within the reservoir (that is, fluid entering the reservoir is instantaneously mixed with the existing fluid). The rate of change of temperature within the reservoir can be computed using

$$\frac{dT_{\text{reservoir}}}{dt} = \frac{\dot{m}_{\text{coolant}}}{m_{\text{coolant}}}(T_{\text{in}} - T_{\text{reservoir}}), \quad (16)$$

where  $T_{\text{reservoir}}$  is the reservoir (and reservoir outlet) temperature,  $\dot{m}_{\text{coolant}}$  is the coolant mass flow rate,  $m_{\text{coolant}}$  is the mass of coolant in the reservoir, and  $T_{\text{in}}$  is the reservoir inflow temperature.

The CoolantReservoir group combines the rate equation (16) with an Integrator to solve for reservoir temperatures at every time point, given an initial temperature. Quasi-steady thermal analysis cannot model the effect of a fluid reservoir, which is purely a thermal mass effect. When  $\dot{m}/m$  becomes large due to a small coolant mass relative to the mass-flow-rate, the time constant associated with the reservoir temperature becomes small. As  $m$  tends to zero we approach the quasi-steady solution. A small time constant makes the thermal ODE very stiff and introduces numerical difficulties in the overall time integration problem.

## 2.5 Refrigeration Cycle

A refrigeration cycle can be used to increase the temperature of “low-quality” waste heat to reject it to the atmosphere with a smaller heat exchanger. This process works similarly to a common household refrigerator, where relatively low-temperature waste heat is raised to a higher temperature so it can be dissipated to the ambient surroundings. For aircraft applications, this refrigeration cycle is often an air-cycle machine (ACM), in which air is used as the working fluid.

The model used in this study was previously described by Jasa et al. [21] and a schematic of the work and heat flow for this simplified cycle is shown in Fig. 2.5-1. The ACM is modeled as a closed-loop Brayton cycle, where the working fluid flows through a low-temperature heat exchanger and accepts input heat, shown as  $Q_c$ . Work ( $W$ ) is then done on the fluid in the compressor, which increases the temperature and pressure of the fluid. This heated fluid then flows through a high-temperature heat exchanger, where the “high-quality” waste heat is rejected, shown as  $Q_h$ . The fluid then goes through a turbine and expands, returning to a low temperature and pressure before returning to the low-temperature heat exchanger.

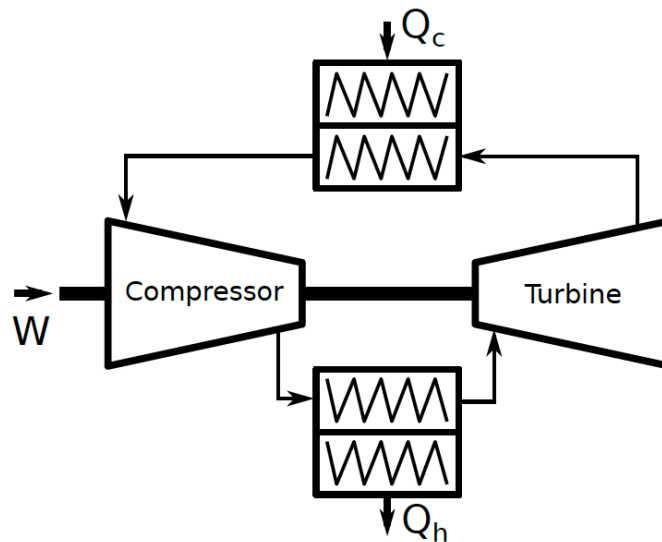


Figure 2.5-1: The refrigeration cycle system [21]

We model the ACM using a system of equations adapted from Moran et al. [23] to capture the relevant physics without adding unnecessary complexity to the model. From the lifting system equations, we get the following expression for the heat load that must be dissipated using the duct heat exchanger:

$$Q_h = \frac{W'}{1 - T_c/T_h} = \frac{\eta_p \eta_f W}{1 - T_c/T_h}, \quad (17)$$

where  $W'$  is the efficiency-adjusted work,  $T_c$  and  $T_h$  are the temperatures of the cooling fluid at the electronics and duct heat exchangers, respectively,  $W$  is the work coming from the shaft,  $\eta_p$  is the shaft power transfer efficiency, and  $\eta_f$  is the friction loss efficiency. We can then solve for the cold-side heat load,  $Q_c$ , and get

$$Q_c = Q_h - (2 - \eta_f) \eta_p W. \quad (18)$$

Using these equations, we can determine the amount of heat transfer on both the hot and cold sides of the lifting system based on the work that is put in. This system is implemented in OpenConcept as the `LiftingSystemComponent`.

## 2.6 Coolant Duct

Ducted radiators greatly reduce cooling drag compared to finned heat sinks in the freestream [24, 25]. There are two primary mechanisms for this. First, a duct that decelerates flow prior to encountering the heat exchanger element generally undergoes a lower total pressure loss. Second, the combination of duct and heat exchanger can act as a weak ramjet providing a further modest offset to the drag of the whole arrangement. For aircraft with high-temperature cooling loads flying at relatively high speeds, a large portion of the drag can be offset. The most famous application of this weak ramjet concept (known as the Meredith effect) is the North American P-51 Mustang's liquid engine cooling system [24].

The user has two options for computing cooling drag due to ducted heat exchangers. The first option is an incompressible approximation. Adapting the method of Theodorsen [25], we model a duct with a frontal opening, diffuser, heat exchanger, and nozzle (Fig. 2.6-1). The fluid density everywhere in the duct is assumed to be  $\rho_\infty$ . Let  $A_{hex}$  be the free flow passage area of the heat exchanger, and  $A_e$  be the exit nozzle area. Let  $\Delta p_{0,hex}$  be the pressure loss across the heat exchanger as a function of the duct mass flow rate  $\dot{m}$ . Let  $\xi_e$  be a static pressure loss as a function of nozzle dynamic pressure, that is  $\Delta p_{0,e} = \xi_e q_e$ . We assume that the nozzle expands the flow back to the freestream static pressure  $p_\infty$ , though this assumption would not hold if a variable-area exit door or cowl flap were used.

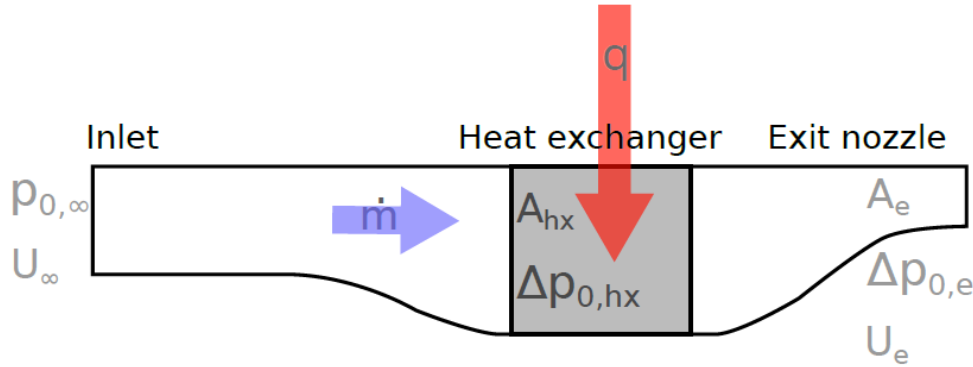


Figure 2.6-1: Ducted heat exchanger to reduce cooling drag

The total pressure at the exit is then computed as:

$$p_{0,e} = p_{0,\infty} - \Delta p_{0,hex} - \Delta p_{0,e} = p_\infty + \frac{1}{2}\rho U_\infty^2 - \Delta p_{0,hex} - \Delta p_{0,e} = p_e + \frac{1}{2}\rho U_e^2 \quad (19)$$

Substituting  $\Delta p_{0,e} = \xi_e (1/2) \rho_\infty U_e^2$  and rearranging we obtain:

$$U_e = \sqrt{\frac{U_\infty^2 - \frac{2}{\rho}((p_e - p_\infty) + \Delta p_{hex})}{1 + \xi_e}}, \quad (20)$$

By continuity:

$$\dot{m} = A_e \rho U_e. \tag{21}$$

We compute net force by balancing the change in fluid momentum ( $\dot{m} \Delta U$ ) and pressure forces. To account for inlet, duct, and nozzle losses not otherwise accounted for, we apply a factor ( $C_{fg} = 0.98$ ) to gross thrust in the drag computation and obtain:

$$F_{net} = \dot{m}(U_e C_{fg} - U_\infty) + A_e C_{fg} (p_e - p_\infty). \tag{22}$$

The incompressible duct computation is implemented as the `ExplicitIncompressibleDuct` component in `OpenConcept`. Alternatively, the `components/ducts` package contains the `ImplicitCompressibleDuct` group, that uses a more sophisticated 1D thermodynamic cycle modeling approach to compute drag. Isentropic relations are used to solve for Mach numbers and flow properties implicitly using `OpenMDAO`'s Newton solver. The compressible model captures Mach number and heat addition effects on net cooling drag. However, the additional fidelity is usually not meaningful for low-speed general aviation airplanes with moderate cooling heat loads, and the compressible relations introduce many implicit states and some robustness issues to the overall MDO problem.

### 3.0 CASE STUDY: REVISITING THE SERIES HYBRID TWIN

To exercise the TMS model and assess the impact of thermal constraints on the design space, we revisit our previous MDO trade space exploration study of a series hybrid twin turboprop [13]. Our baseline aircraft is a Beechcraft King Air C90GT with a drop-in replacement series-hybrid propulsion system replacing the turboprop engines.

The series-hybrid electric propulsion architecture is illustrated in Fig. 3-1. To enable the aircraft to continue safe flight and landing after loss of any single component on takeoff, the propulsion system uses two electric motors, two propellers, and a battery large enough to provide full takeoff power in the event of engine loss. These features should provide the same level of redundancy of the conventional twin turboprop configuration. Specific power, efficiency, and cost assumptions for individual powertrain components are listed in Table 3-1.

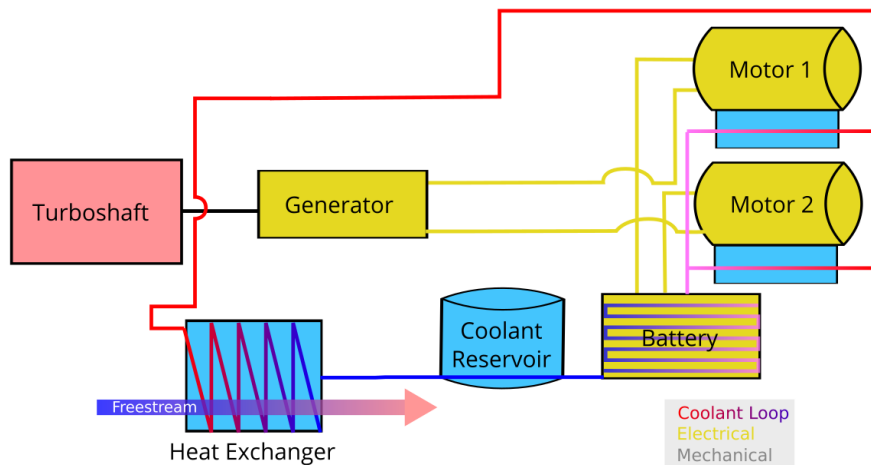


Figure 3-1: Systems architecture for the twin series hybrid case study

**Table 3-1: Powertrain technology assumptions [13]**

Component	Specific Power (kW/kg)	Efficiency	PSFC (lb/hp/hr)
<b>Battery</b>	5.0	97%	--
<b>Motor</b>	5.0	97%	--
<b>Generator</b>	5.0	97%	--
<b>Turboshaft</b>	7.15*	--	0.6

\*Not including 104kg base weight

### 3.1 Mission Analysis Methodology

To compute mission fuel burn and other performance constraint values, we perform a full mission analysis at every MDO iteration consisting of a balanced-field takeoff (with loss of one propulsor at the  $V_1$  speed), climb, cruise, and descent. We use the same mission analysis methodology as our previous work [13], with the exception noted below. OpenConcept’s balanced field takeoff length computation consists of two branched trajectories composed of five piecewise segments:

1. Takeoff roll at full power from  $V_0$  to  $V_1$
2. Takeoff roll at one-engine-inoperative (OEI) power from  $V_1$  to  $V_R$
3. Rejected takeoff with zero power and maximum braking from  $V_1$  to  $V_0$
4. Transition in a steady circular arc to the OEI climb-out flight path angle and speed
5. Steady climb at  $V_2$  speed and OEI power until an obstacle height  $h_o$  is reached

We compute the balanced field takeoff by varying  $V_1$  until the accelerate-go distance (segments 1, 2, 4, and 5) is at least as long as the accelerate-stop distance (segments 1 and 3).

During the takeoff roll (segments 1, 2, and 3), the force balance equation is:

$$\frac{d\vec{V}}{dt} = \vec{T} - \vec{D} - \mu(m\vec{g} - \vec{L}). \quad (23)$$

In our previous work, we had used a method that integrates segments 1, 2, and 3 with respect to velocity instead of time [26]. The advantage of this method is that it exhibits good numerical stability; however, it cannot be used to integrate general ODEs including the thermal models of Section 2. During the takeoff roll, the airplane is producing maximum heat and has minimum ability to reject the heat. Therefore, instead of neglecting heating during takeoff, we changed to a time-based integration scheme capable of computing accurate time histories of all parameters. Times, distances, and altitudes for segments 4 and 5 are computed using prescribed kinematics from Raymer [26]; however, we time-integrate all the other states, including thermal loads and battery state.

The climb, cruise, and descent segments are computed using steady flight equations. At each flight condition, the Newton solver sets a throttle parameter such that the following residual equation is satisfied:

$$\vec{R}_{\text{thrust}} = \vec{T} - \vec{D} - \vec{m}g \sin(\vec{\gamma}). \quad (24)$$

The user specifies the true airspeed and the vertical speed at each mission point, as well as one constraint per mission segment (e.g., an altitude for top of climb or mission range for cruise). OpenMDAO then computes the segment duration required to satisfy the constraints for climb, cruise, and descent using the Newton

solver. OpenConcept integrates range, altitude, fuel flow, battery SOC, and all other thermal states.

Cruise drag is computed using a drag polar with constant coefficients. We assumed an Oswald efficiency  $e = 0.8$  and matched computed range to published range for a design mission by setting  $C_{D0} = 0.022$ . Weights are computed parametrically based on wing area, aspect ratio, MTOW, and other high-level parameters. The empty weight was calibrated to match the King Air C90GT baseline by matching our model's parametric operating empty weight (OEW) to the published OEW (minus engine weight in both cases) by applying a factor of 2.0 to our model's computed structural weight (based on rough textbook formulas).

### 3.2 Optimization Without Thermal Constraints

We begin by re-running the series hybrid twin tradespace exploration from our previous work [13]. We are interested in the optimal aircraft design at a variety of battery technology levels (quantified by the specific energy,  $e_b$ ) and design mission ranges. Therefore, we run a grid of MDO problems formulated as follows:

minimize: fuel burn + 0.01 MTOW

by varying:

MTOW

$S_{ref}$

$d_{prop}$

$W_{battery}$

$P_{motor}$  (rated)

$P_{turboshaft}$  (rated)

$P_{generator}$  (rated)

$H_E$  (degree of hybridization with respect to energy)

subject to scalar constraints

$$R_{TOW} = W_{TO} - W_{fuel} - W_{empty} - W_{payload} - W_{batt} \geq 0$$

$$R_{batt} = E_{batt,max} - E_{batt,used} \geq 0$$

$$R_{vol} = W_{fuel,max} - W_{fuel} \geq 0$$

$$BFL \leq 4452 \text{ ft (no worse than baseline)}$$

$$\text{engine-out climb gradient} \geq 2\%$$

$$V_{stall} \leq 81.6 \text{ kts (no worse than baseline)}$$

and vector constraints:

$$P_{motor} \leq 1.05 P_{motor} \text{ (rated)}$$

$$P_{turboshaft} \leq P_{turboshaft} \text{ (rated)}$$

$$P_{generator} \leq P_{generator} \text{ (rated)}$$

$$P_{battery} \leq W_{battery} p_b$$

The objective function was chosen in order to prioritize reducing tailpipe carbon emissions. However, certain combinations of specific energy and range result in aircraft with zero fuel burn. Optimizing for fuel burn alone in these cases is an ill-posed problem. Therefore, we add a small contribution of MTOW to the objective function in order to force the optimizer to design reasonable all-electric aircraft. A potentially better objective function would be to minimize total carbon emissions. This approach introduces location dependence into the problem, since electricity is generated using more or less carbon-intensive methods in different parts of the world. The vectorial constraint quantities represent parameters tracked over time during a mission. Each entry in the vector represents an individual point in time. Each mission segment (climb, cruise and descent) consists of 10 discrete time intervals.

We optimized one airplane at each combination of specific energy (from 250 to 800 Wh/kg) and design range (300 to 700 nautical miles). Each airplane flew with the same climb, cruise, and descent speeds (both

indicated airspeed and vertical speed). We used the `scipy.optimize` implementation of the SLSQP optimization algorithm to solve the problem.

The results are similar to the previous study despite some changes to the mission analysis methods. Figure 3.2-1 exhibits the same multimodal tradespace as we found before. At long ranges and poor  $e_b$ , little battery is used (only enough to provide backup power on takeoff) and the airplane is essentially turboelectric. At short range and high  $e_b$ , the mission is flown entirely on battery and no fuel is used. In between these two extremes, the optimizer prefers to use all of the allotted maximum takeoff weight until it hits the upper bound (5700 kg), above which a type rating is required in many jurisdictions including the United States and European Union.

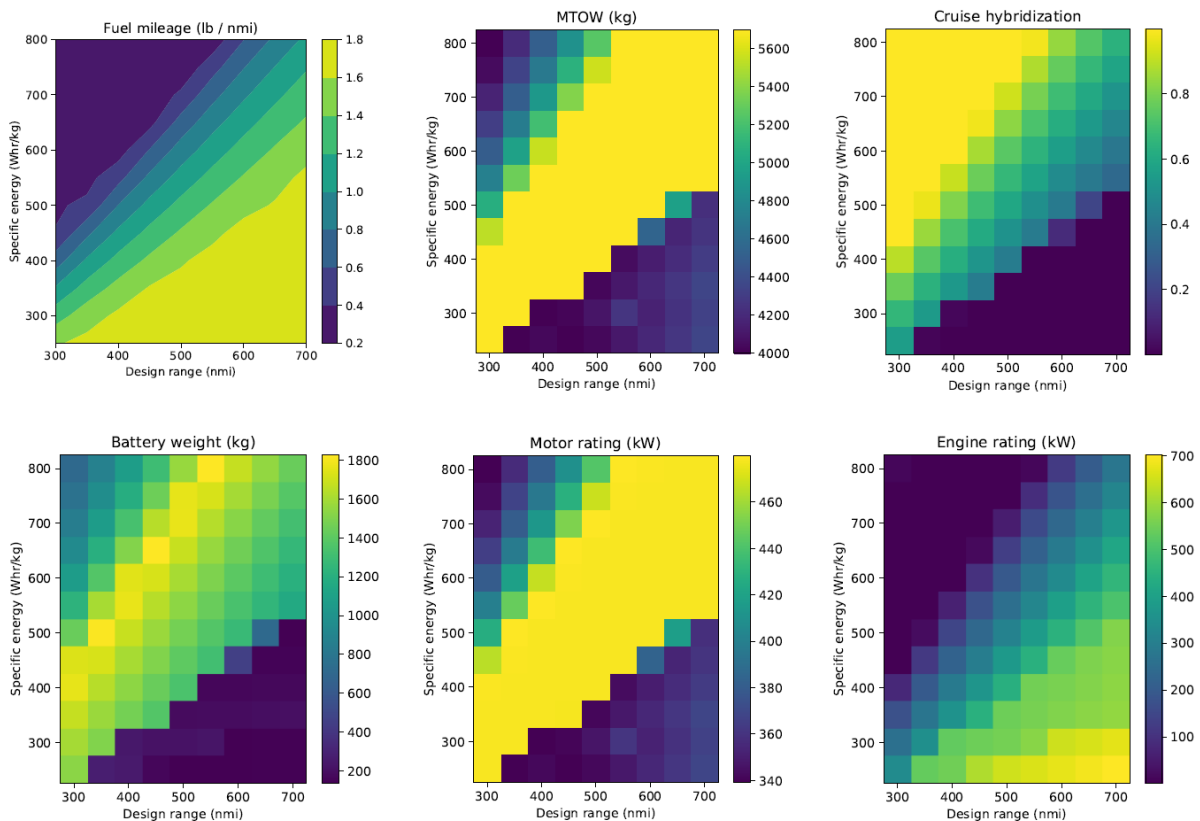


Figure 3.2-1: Minimum fuel burn MDO results without thermal constraints

### 3.3 Optimization with Thermal Constraints

In this work, we modified the aircraft propulsion model to include thermal management of the motor and battery. We added a `ThermalComponentWithMass` to the motor (lumping both motors together) and to the battery pack. Thermal mass of both components was computed using a specific heat of 921 J/kg/K (representative of aerospace-grade aluminum). We connected cold plates of both components in series using a liquid cooling system using a propylene glycol and water mixture with a specific heat of 3801 J/kg/K [27]. The coolant loop rejects heat via a ducted heat exchanger. We neglect the drag-offsetting effect of heat addition and use an `ExplicitIncompressibleDuct` to model the air mass flow and drag. We use OpenConcept's default geometric parameters for the offset strip fin heat exchanger. Finally, we include a liquid coolant reservoir upstream of the heat exchanger. We include the weight of the coolant and heat exchanger in the empty weight of the airplane, and include the drag contribution of the duct and heat exchanger. Figure 3.3-1 shows profiles of mission parameters for a single aircraft design at 250 Wh/kg and

400 nmi range. The figure highlights the importance of time-accurate thermal analysis. During takeoff and low-altitude climb, heating is at its maximum and convective heat transfer capability is at a minimum (due to higher atmospheric temperature and lower coolant duct mass flow). A quasi-steady thermal analysis would predict very high temperatures during this part of the mission. However, because the thermal components have considerable thermal mass, the maximum temperature is not reached until the top of the climb phase. Sizing the thermal management system to a quasi-steady analysis at the most critical condition (early in the takeoff roll) would result in an oversized heat exchanger and unnecessarily high drag and weight penalty.

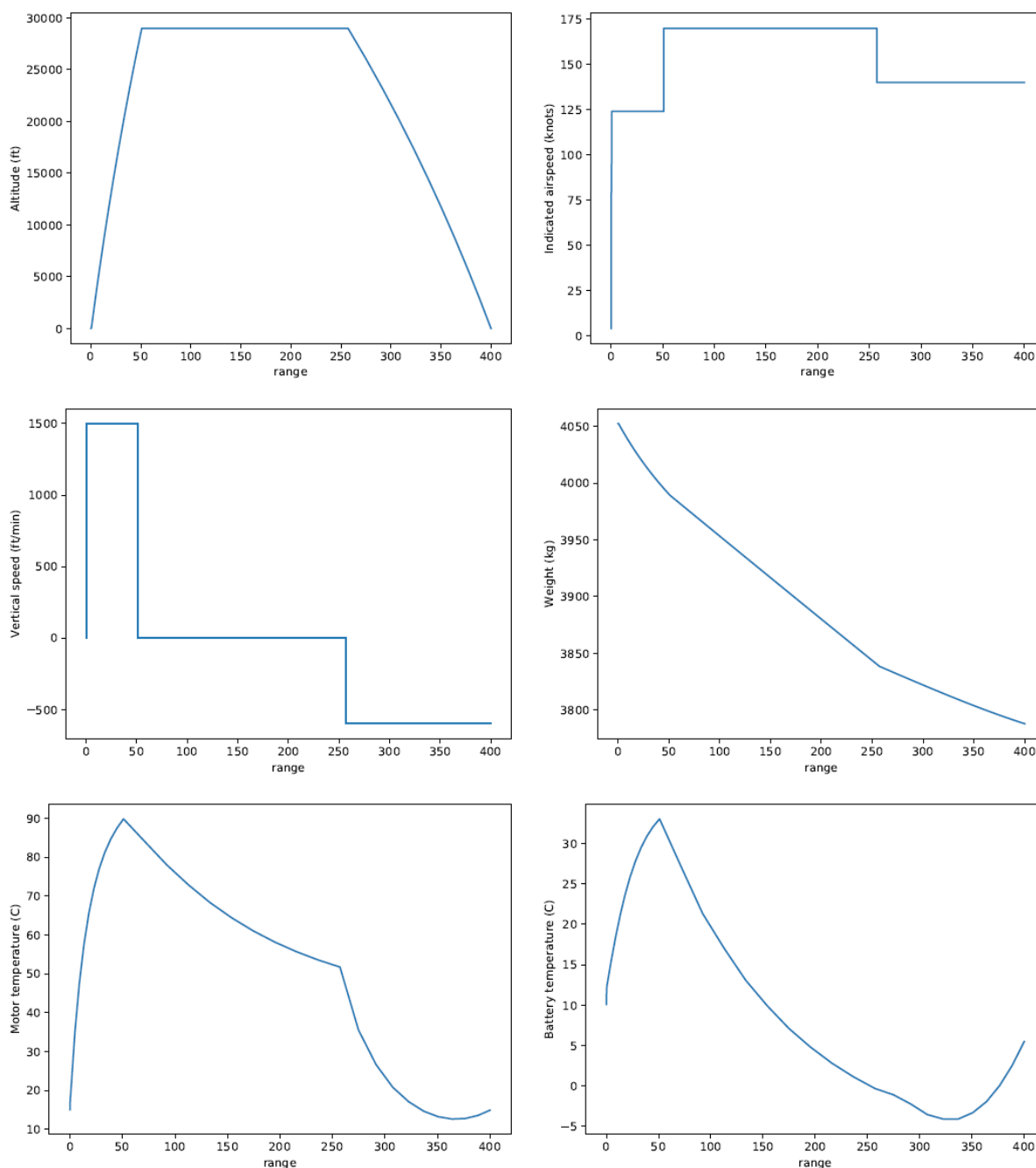


Figure 3.3-1: Mission trajectories for a 400 nmi mission ( $e_b = 250$ )

We also add several design variables and constraints to the previous problem. We let the optimizer size the

heat exchanger width and area of the duct nozzle, thus allowing it to trade off weight and drag for equal heat rejection capability. We also allow the optimizer to size the coolant reservoir. We constrain the time-accurate temperatures of the motor and battery pack to stay within operating limits (90° C for the motor and 50° C for the battery). The full MDO problem is as follows:

minimize: fuel burn + 0.01 MTOW  
 by varying:

- MTOW
- $S_{ref}$
- $d_{prop}$
- $W_{battery}$
- $P_{motor}$  (rated)
- $P_{turboshaft}$  (rated)
- $P_{generator}$  (rated)
- $H_E$  (degree of hybridization with respect to energy)
- $A_{nozzle}$  (cooling duct outlet cross-sectional area)
- $n_{wide}$  (number of heat exchanger cells wide)
- $m_{coolant}$  (coolant reservoir mass)

subject to scalar constraints

- $R_{TOW} = W_{TO} - W_{fuel} - W_{empty} - W_{payload} - W_{batt} \geq 0$
- $R_{batt} = E_{batt,max} - E_{batt,used} \geq 0$
- $R_{vol} = W_{fuel,max} - W_{fuel} \geq 0$
- BFL  $\leq$  4452 ft (no worse than baseline)
- engine-out climb gradient  $\geq$  2%
- $V_{stall} \leq$  81.6 kts (no worse than baseline)

and vector constraints:

- $P_{motor} \leq 1.05 P_{motor}$  (rated)
- $P_{turboshaft} \leq P_{turboshaft}$  (rated)
- $P_{generator} \leq P_{generator}$  (rated)
- $P_{battery} \leq W_{battery} p_b$
- $T_{motor} \leq 90^\circ \text{ C}$
- $T_{battery} \leq 50^\circ \text{ C}$

Figure 3.3-2 shows the design variables and selected responses at the optimal points across the trade space. The motor temperature constraint is always active at the top of climb for all the designs in the tradespace (and so is not shown in Fig. 3.3-2). The optimizer varies the duct nozzle area (to vary cooling air mass flow) and motor size (to add thermal mass) such that the motor temperature reaches the limit at the top of the climb. The heat exchanger width converges to its upper bound at virtually every point in the design space, while coolant mass converges to its lower bound at every point.

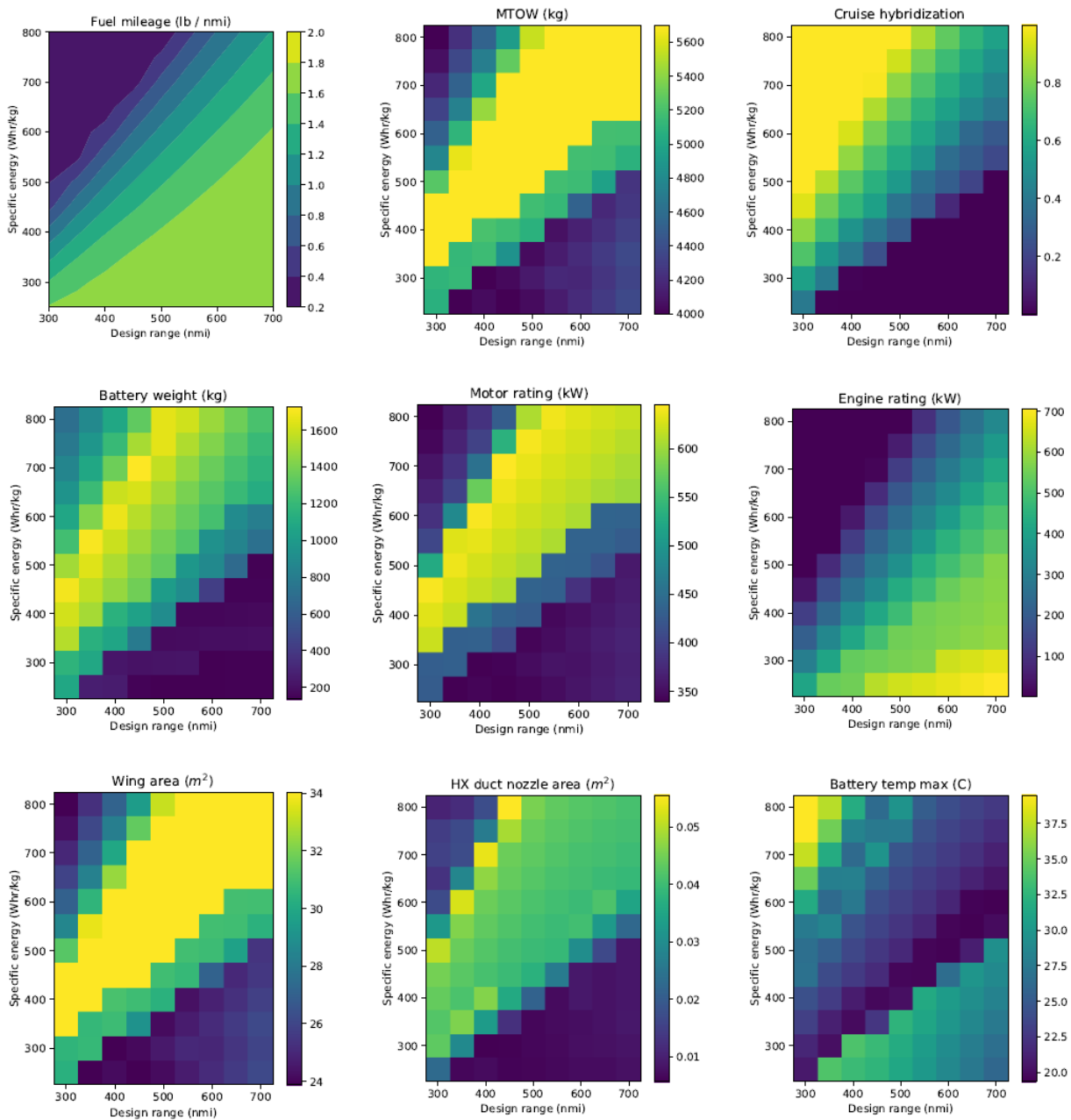
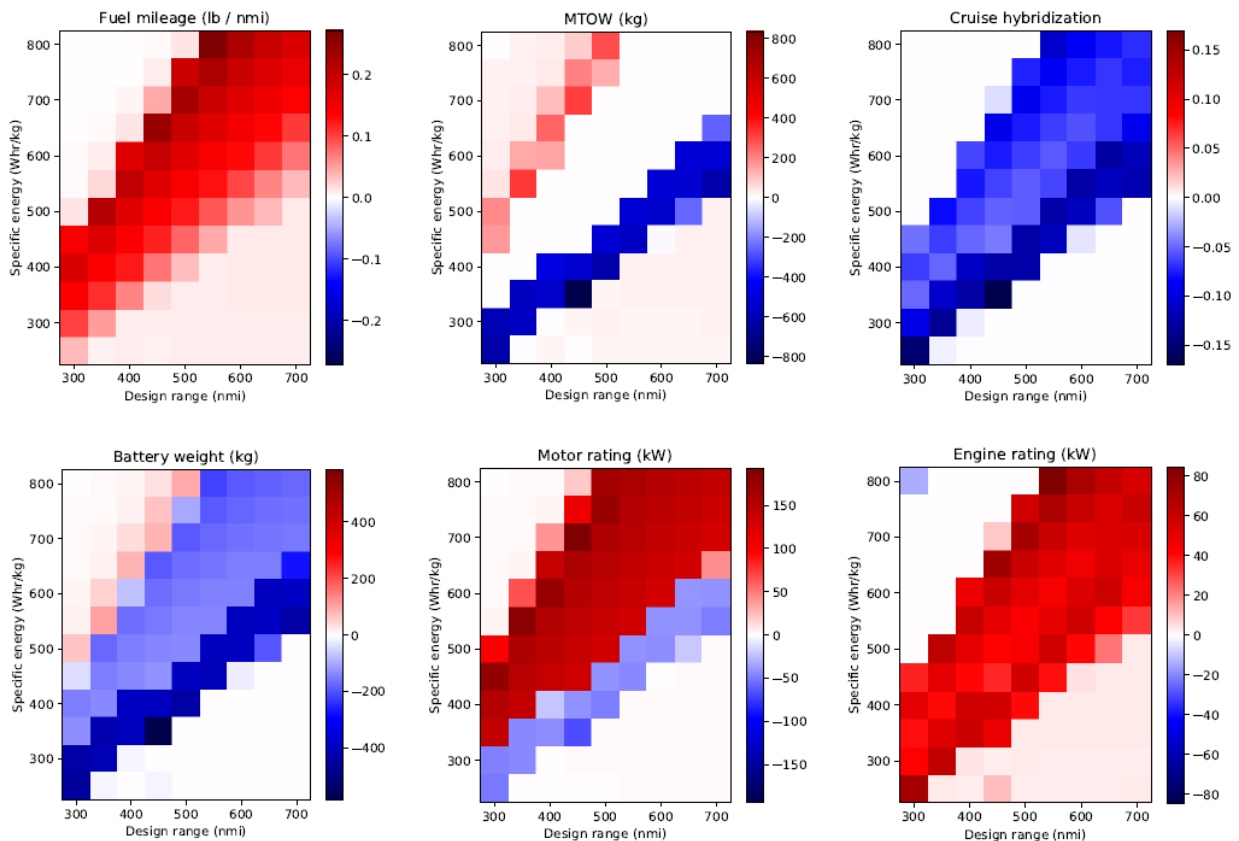


Figure 3.3-2: Minimum fuel burn MDO results with thermal constraints

Figure 3.3-3 shows the difference in key variables (including fuel mileage) after accounting for thermal design and thermal constraints. While fuel mileage worsened at every point in the design space, the impact was much larger on certain combinations of specific energy and design range. At long range and low battery specific energy, and at short range and high specific energy, there was little effect. The long-range designs with low  $e_b$  are essentially turboelectric and benefit from light weight and low battery waste heat; there is simply less overall heat to reject, thus minimizing the associated penalty. The short-range designs with high  $e_b$  use no fuel to begin with, so their fuel burn remains at zero even as they use more energy; instead, we see the thermal management penalty as an increase in MTOW. Between these two extreme designs, the heavy hybrid airplanes generate a large amount of waste heat and burn appreciable fuel, making the impact of

thermal constraints more significant.



**Figure 3.3-3: Difference in optimal designs due to thermal constraints  
(positive = thermally-constrained higher)**

A very interesting trend emerged in the motor sizing design variable. The optimizer greatly oversized the motors in a band in the heart of the tradespace (seen as a band of red from middle left to top right). In the rest of the tradespace, the motor is sized by power required during climb. However, in the red band, the motor is being constrained by the thermal problem. We suspect that this is a result of the sequencing of components in the thermal management system. We designed the TMS architecture to provide the coldest coolant to the battery, since it has a lower operating temperature. The consequence is that warmer coolant flows into the motor. The motor inflow temperature varies slowly even as outside temperature drops due to the thermal mass of the battery. The best solution available to the optimizer is to oversize the motors to add thermal mass and avoid overheating at the critical top of climb point. Reordering the components may result in an improvement in fuel burn in this part of the tradespace by better balancing peak temperatures between the motor and battery.

## 4.0 CONCLUSIONS

Thermal constraints are currently understudied compared to other disciplines in aircraft conceptual design, and there are few publicly-available resources available for the research community to incorporate thermal constraints into electric aircraft studies. To fill this gap, we introduced thermal analysis and design capabilities within the OpenConcept Python package. We demonstrate that thermal mass effects are significant when analyzing aircraft thermal trajectories, particularly early in the mission when power is high and speeds and altitudes are low. Therefore, pseudo-steady thermal models are not sufficient for the design

of aircraft thermal management systems, because they can lead to dramatic over-sizing. We integrated time-accurate thermal models into the mission analysis and used them to formulate constraints in the aircraft design optimization problem. The time-accurate thermal analyses and derivatives were computed by the OpenConcept package to enable efficient gradient-based design optimization.

We showed that thermal constraints appreciably affect the fuel burn and energy usage achievable in a series hybrid architecture, but not uniformly throughout the tradespace. The non-uniform effects make the impact of thermal constraints on aircraft design somewhat non-intuitive and underscore the importance of including them early in the design process. Electric aircraft architectures with a large percentage of battery power will be impacted by TMS penalties, but because they burn little or no fuel, the penalty is seen as an MTOW and total energy increase, not a fuel burn penalty. Conversely, turboelectric aircraft experience a modest TMS penalty due to lighter weight and lack of battery heating. Hybrid-electric aircraft see the largest fuel burn penalty since they are heavier than turboelectric aircraft (thus producing more motor waste heat) and use significant quantities of batteries (producing yet more waste heat). We also observed that the optimizer can find creative ways to satisfy the thermal constraints (such as oversizing a motor to add thermal mass and avoid a transient over-temperature condition).

## **ACKNOWLEDGEMENT**

The first and second authors were supported by the National Science Foundation Graduate Research Fellowship Program under Grant DGE 1256260. Any opinions, findings, and conclusions or recommendations expressed in this material are those of the authors and do not necessarily reflect the views of the National Science Foundation. The fourth author was supported by NASA ARMD's Transformational Tools and Technologies project. This work was also supported by the U.S. Air Force Research Laboratory (AFRL) under the Michigan-AFRL Collaborative Center in Aerospace Vehicle Design (CCAVID), with Richard Snyder as the task Technical Monitor.

## REFERENCES

- [1] Trawick, D., Perullo, C. A., Armstrong, M. J., Snyder, D., Tai, J. C., and Mavris, D. N., “Development and Application of GT-HEAT for the Electrically Variable Engine Design,” 55th AIAA Aerospace Sciences Meeting, Grapevine, TX, 2017. doi:10.2514/6.2017-1922, URL <http://arc.aiaa.org/doi/10.2514/6.2017-1922>.
- [2] Falck, R. D., Chin, J., Schnulo, S. L., Burt, J. M., and Gray, J. S., “Trajectory Optimization of Electric Aircraft Subject to Subsystem Thermal Constraints,” 18th AIAA/ISSMO Multidisciplinary Analysis and Optimization Conference, Denver, CO, 2017. doi:10.2514/6.2017-4002, URL <https://arc.aiaa.org/doi/10.2514/6.2017-4002>.
- [3] Hwang, J. T., and Ning, A., “Large-scale multidisciplinary optimization of an electric aircraft for on-demand mobility,” 2018 AIAA/ASCE/AHS/ASC Structures, Structural Dynamics, and Materials Conference, Kissimmee, FL, 2018, pp. 1–18. doi:10.2514/6.2018-1384, URL <https://arc.aiaa.org/doi/abs/10.2514/6.2018-1384>.
- [4] Antcliff, K. R., Guynn, M. D., Marien, T., Wells, D. P., Schneider, S. J., and Tong, M. T., “Mission Analysis and Aircraft Sizing of a Hybrid-Electric Regional Aircraft,” 54th AIAA Aerospace Sciences Meeting, San Diego, CA, 2016, pp. 1–18. doi:10.2514/6.2016-1028, URL <http://arc.aiaa.org/doi/10.2514/6.2016-1028>.
- [5] Vratny, P. C., Gologan, C., Pernet, C., Isikveren, A. T., and Hornung, M., “Battery Pack Modeling Methods for Universally- Electric Aircraft,” 4th CEAS Air and Space Conference, Linkoping, Sweden, 2013.
- [6] Wroblewski, G. E., and Ansell, P. J., “Mission Analysis and Emissions for Conventional and Hybrid-Electric Commercial Transport Aircraft,” 2018 AIAA Aerospace Sciences Meeting, Kissimmee, FL, 2018. doi:10.2514/6.2018-2028, URL <https://doi.org/10.2514/6.2018-2028>.
- [7] Cipolla, V., and Oliviero, F., “HyPSim : A Simulation Tool for Hybrid Aircraft Performance Analysis,” Variational Analysis and Aerospace Engineering, 2016, pp. 95–116. doi:10.1007/978-3-319-45680-5.
- [8] Welstead, J. R., Caldwell, D., Condotta, R., and Monroe, N., “An Overview of the Layered and Extensible Aircraft Performance System (LEAPS) Development,” 2018 AIAA Aerospace Sciences Meeting, Kissimmee, FL, 2018. doi:10.2514/6.2018-1754.
- [9] Capristan, F. M., and Welstead, J. R., “An Energy-Based Low-Order Approach for Mission Analysis of Air Vehicles in LEAPS,” 2018 AIAA Aerospace Sciences Meeting, Kissimmee, FL, 2018. doi:10.2514/6.2018-1755, URL <https://arc.aiaa.org/doi/10.2514/6.2018-1755>.
- [10] Vegh, J. M., Alonso, J. J., Orra, T. H., and Ilario da Silva, C. R., “Flight Path and Wing Optimization of Lithium-Air Battery Powered Passenger Aircraft,” 53rd AIAA Aerospace Sciences Meeting, Kissimmee, FL, 2015. doi:10.2514/6.2015-1674, URL <http://dx.doi.org/10.2514/6.2015-1674>.
- [11] Lents, C. E., Hardin, L. W., Rheume, J., and Kohlman, L., “Parallel Hybrid Gas-Electric Geared Turbofan Engine Conceptual Design and Benefits Analysis,” 52nd AIAA/SAE/ASEE Joint Propulsion Conference, Salt Lake City, UT, 2016. doi:10.2514/6.2016-4610, URL <http://dx.doi.org/10.2514/6.2016-4610>.
- [12] Freeman, J., Osterkamp, P., Green, M. W., Gibson, A. R., and Schiltgen, B. T., “Challenges and opportunities for electric aircraft thermal management,” Aircraft Engineering and Aerospace Technology, Vol. 86, No. 6, 2014, pp. 519–524. doi: 10.1108/AEAT-04-2014-0042, URL <http://www.emeraldinsight.com/doi/10.1108/AEAT-04-2014-0042>.

- [13] Brelje, B. J., and Martins, J. R. R. A., “Development of a Conceptual Design Model for Aircraft Electric Propulsion with Efficient Gradients,” Proceedings of the AIAA/IEEE Electric Aircraft Technologies Symposium, Cincinnati, OH, 2018. doi:10.2514/6.2018-4979.
- [14] Gray, J. S., Hwang, J. T., Martins, J. R. R. A., Moore, K. T., and Naylor, B. A., “OpenMDAO: An open-source framework for multidisciplinary design, analysis, and optimization,” Structural and Multidisciplinary Optimization, Vol. 59, No. 4, 2019, pp. 1075–1104. doi:10.1007/s00158-019-02211-z.
- [15] Schnulo, S. L., Chin, J., Smith, A. D., and Dubois, A., “Steady State Thermal Analyses of SCEPTOR X-57Wingtip Propulsion,” 17th AIAA Aviation Technology, Integration, and Operations Conference, Denver, CO, 2017, pp. 1–14.
- [16] Schnulo, S. L., Jeff Chin, R. D. F., Gray, J. S., Papathakis, K. V., Clarke, S. C., Reid, N., and Borer, N. K., “Development of a Multi-Segment Mission Planning Tool for SCEPTOR X-57,” 2018 Multidisciplinary Analysis and Optimization Conference, AIAA, Atlanta, GA, 2018. doi:10.2514/6.2018-3738.
- [17] Chin, J., Schnulo, S. L., Miller, T., Prokopius, K., and Gray, J. S., “Battery Performance Modeling on SCEPTOR X-57 Subject to Thermal and Transient Considerations,” AIAA Scitech 2019 Forum, AIAA, San Diego, CA, 2019. doi:10.2514/6.2019-0784.
- [18] Falck, R. D., Chin, J. C., Schnulo, S. L., Burt, J. M., and Gray, J. S., “Trajectory Optimization of Electric Aircraft Subject to Subsystem Thermal Constraints,” 18th AIAA/ISSMO Multidisciplinary Analysis and Optimization Conference, Denver, CO, 2017.
- [19] Incropera, F. P., Fundamentals of Heat and Mass Transfer, John Wiley and Sons, Inc., USA, 2006.
- [20] Kays, W., and London, A., Compact Heat Exchangers, Third Edition, McGraw-Hill Book Company, 1984.
- [21] Jasa, J. P., Brelje, B. J., Mader, C. A., and Martins, J. R. R. A., “Coupled Design of a Supersonic Engine and Thermal System,” World Congress of Structural and Multidisciplinary Optimization, Beijing, China, 2019.
- [22] Manglik, R. M., and Bergles, A. E., “Heat Transfer and Pressure Drop Correlations for the Rectangular Offset Strip Fin Compact Heat Exchanger,” Experimental Thermal and Fluid Science, 1995, pp. 171–180. doi:10.1016/0894-1777(94)00096-Q.
- [23] Moran, M. J., Shapiro, H. N., Boettner, D. D., and Bailey, M. B., Fundamentals of engineering thermodynamics, John Wiley & Sons, 2010.
- [24] Meredith, F. W., “Cooling of aircraft engines with special reference to ethylene glycol radiators enclosed in ducts,” Tech. Rep. 1683, Government of the United Kingdom Air Ministry Reports and Memoranda, 1935.
- [25] Theodorsen, T., “The Fundamental Principles of the N.A.C.A. Cowling,” Journal of the Aeronautical Sciences, Vol. 5, No. 5, 1938, pp. 169–174. doi:10.2514/8.566.
- [26] Raymer, D. P., Aircraft Design: A Conceptual Approach, 5th ed., AIAA, 2012.
- [27] The Dow Chemical Company, “DOWFROST Technical Data Sheet”, 2019.